

TIME-DEPENDENT MODELING OF GAMMA-RAY FLARES IN BLAZAR PKS 1510–089

S. SAITO^{1,2}, L. STAWARZ^{3,2}, Y. T. TANAKA⁴, T. TAKAHASHI², M. SIKORA⁵, R. MODERSKI⁵

Draft version September 5, 2018

ABSTRACT

Here we present a new approach for constraining luminous blazars, incorporating fully time-dependent and self-consistent modeling of bright γ -ray flares of PKS 1510–089 resolved with *Fermi*-LAT, in the framework of the internal shock scenario. The results of our modeling imply the location of the γ -ray flaring zone outside of the broad-line region, namely around $\simeq 0.3$ pc from the core for a free-expanding jet with the opening angle $\Gamma\theta_{\text{jet}} \simeq 1$ (where Γ is the jet bulk Lorentz factor), up to $\simeq 3$ pc for a collimated outflow with $\Gamma\theta_{\text{jet}} \simeq 0.1$. Moreover, under the $\Gamma\theta_{\text{jet}} \simeq 1$ condition, our modeling indicates the maximum efficiency of the jet production during the flares, with the total jet energy flux strongly dominated by protons and exceeding the available accretion power in the source. This is in contrast to the quiescence states of the blazar, characterized by lower jet kinetic power and an approximate energy equipartition between different plasma constituents. We demonstrate how strictly simultaneous observations of flaring PKS 1510–089 at optical, X-ray, and GeV photon energies on hourly timescales, augmented by extensive simulations as presented in this paper, may help to impose further precise constraints on the magnetization and opening angle of the emitting region. Our detailed modeling implies in addition that a non-uniformity of the Doppler factor across the jet, caused by the radial expansion of the outflow, may lead to a pronounced time distortion in the observed γ -ray light curves, resulting in particular in asymmetric flux profiles with substantially extended decay phases.

Subject headings: acceleration of particles — radiation mechanisms: non-thermal — galaxies: active — galaxies: jets — quasars: individual (PKS 1510–089) — gamma rays: galaxies

1. INTRODUCTION

Blazars constitute a population of radio-loud Active Galactic Nuclei (AGN) with relativistic jets directed toward the Earth. The observed spectrum of a blazar is dominated by the jet component as a result of a strong relativistic beaming involved, and consists of the two broad humps in the $\nu - \nu F_\nu$ representation (hereafter the ‘spectral energy distribution’, SED). The low energy hump, peaked in the infrared-to-X-ray frequency range, is due to the synchrotron emission of ultra-relativistic jet electrons, while the high energy component, peaking in the γ -ray band, originates from the inverse Compton radiation of relativistic electrons interacting with ambient seed photons produced either externally to the jet (predominantly via a re-processing of the accretion disk emission by the circumnuclear gas and dust), or within the outflow by the synchrotron process.

Blazars can be classified as either BL Lacertae objects (BL Lacs) or flat-spectrum radio quasars (FSRQs), based on the properties of the optical line emission. In particular, the latter class of sources is characterized by the presence of prominent broad and narrow emission lines in their spectra. FSRQs constitute the most luminous

population of blazars, with super massive black holes (SMBHs) accreting at high rates (over 1% of the Eddington limit; e.g., Sbarrato et al. 2014). The available huge accretion mass flux is converted very efficiently to the jet energy flux within the ergospheres of rapidly spinning SMBHs at the expense of the black hole rotational energy (Blandford & Znajek 1977; Sikora et al. 2007; Tchekhovskoy et al. 2011). In this context, high-energy observations are indispensable for imposing meaningful constraints on the jet energetics, since the bulk of the radiative energy of luminous blazars is released in the MeV/GeV range (see Ghisellini et al. 2014). And indeed, it was repeatedly shown that the amount of the jet power dissipated radiatively during the flares of FSRQs in γ -rays is often comparable to the corresponding disk luminosities (Tanaka et al. 2011; Saito et al. 2013).

Blazars display complex variability patterns on various timescales across the entire electromagnetic spectrum, with high-amplitude flux changes pronounced most clearly at high frequencies. The all-sky γ -ray survey with the Large Area Telescope onboard the *Fermi* satellite (hereafter *Fermi*-LAT) unveiled in particular very rapid flares of FSRQs in the GeV range, with the observed flux doubling timescales of the order of hours, down to even sub-hour domain in a few cases (see the analysis of the LAT data for PKS 1510–089, 3C 273, and 4C 21.35 by Foschini et al. 2011, 2013; Saito et al. 2013; Brown 2013; Rani et al. 2013). Such a dramatic γ -ray variability indicates a very efficient energization of the jet electrons taking place in compact regions of the enhanced energy dissipation, followed by the rapid radiative cooling of the accelerated particles.

The exact site and structure of those energy dissipa-

s.saito@rikkyo.ac.jp

¹ Department of Physics, Rikkyo University, 3-34-1 Nishi-Ikebukuro, Toshima-ku, Tokyo 171-8501, Japan

² Institute of Space and Astronautical Science JAXA, 3-1-1 Yoshinodai, Chuo-ku, Sagami-hara, Kanagawa 252-5210, Japan

³ Astronomical Observatory, Jagiellonian University, ul. Orla 171, 30-244 Kraków, Poland

⁴ Hiroshima Astrophysical Science Center, Hiroshima University, 1-3-1 Kagamiyama, Higashi-Hiroshima 739-8526, Japan

⁵ Nicolaus Copernicus Astronomical Center, Bartycka 18, 00-716 Warsaw, Poland

tion regions is, however, still controversial, in spite of the extensive broad-band observations carried out over the last two decades. This reflects in a wide range of the estimated position of the blazar emission zone along the jet, even for the same object, based on different sets of observables interpreted in the frameworks of different jet emission models. For example, as for PKS 1510–089, the combined radio, optical polarization, and γ -ray monitoring suggested the dominant emitting region to be located as far as ~ 10 pc from the central SMBH (the “far-dissipation zone” scenario; e.g., Marscher et al. 2010; Orienti et al. 2013). Meanwhile, another studies based on the SED modeling including the UV, X-ray, and γ -ray data, placed the blazar zone in the source at sub-pc distances from the central engine (the “near-dissipation zone” scenario; e.g., Kataoka et al. 2008; Ghisellini et al. 2010). Complex multi-zone/multi-component models were also proposed in order to explain broad-band variability and spectral properties of PKS 1510–089 (Nalewajko et al. 2012a; Aleksić et al. 2014).

In principle, timing characteristics of high-amplitude blazar flares can offer some clues on the location of the active emission zone. First, due to the causality requirement, the linear size of the emission region may be constrained as $r \lesssim c\delta\tau_d/(1+z)$, for the observed flux doubling timescale τ_d and the Doppler factor of the emitting plasma δ . Assuming further a conical, uniform, and free-expanding jet, whose (small) half-opening angle $\theta_{\text{jet}} \simeq r/R$ is approximately the inverse of the jet bulk Lorentz factor Γ , the location of the flaring zone from the central SMBH reads as $R \lesssim c\Gamma\delta\tau_d/(1+z)$. The flux doubling timescale of about a few hours, for example, often inferred for FSRQs from the LAT data as mentioned above, gives therefore $R \lesssim 10^{16}$ cm for the typically expected in blazar sources $\Gamma \simeq \delta \sim 10$, or $R < 10^3 R_S$ in the units of the Schwarzschild radius R_S for the black hole mass of the order of $10^8 M_\odot$. This would be then consistent with the “near-dissipation zone” scenario.

On the other hand, the most recent detections of very high energy γ -rays (photon energies > 100 GeV) from some FSRQs, including PKS 1510–089 (Abramowski et al. 2013; Aleksić et al. 2014; Barnacka et al. 2014), have challenged the above conclusion. That is because such γ -rays are expected to undergo an efficient annihilation in the interactions with lower-energy circumnuclear photon fields, and in particular with the UV disk emission re-processed within the “broad line region” (BLR), if produced at the scales below the characteristic radius of the BLR clouds (~ 0.1 pc for the typical disk luminosity of the order of 10^{46} erg s $^{-1}$; see, e.g., Moderski et al. 2003; Liu & Bai 2006; Tavecchio & Mazin 2009; Barnacka et al. 2014). The detection of very high energy γ -rays from FSRQs seems therefore to require the dominant emission region to be located at larger distances from the core, at least in the framework of the one-zone emission models.

An important issue, which is currently overlooked in the blazar modeling, but which, in fact, is crucial for constraining luminous blazars, is the exact γ -ray spectral evolution during the rapid flux changes, along with the exact time profiles of the flares. *Fermi*-LAT observations of the brightest FSRQs have revealed that spectral breaks appear around a few/several GeV during the enhanced activity states, and that the low- and high-energy

TABLE 1
 γ -RAY FLARING EVENTS OF PKS 1510–089 MODELED IN THIS WORK

Name	MJD (1)	$F_{>100 \text{ MeV}}$ (2)	Γ_γ (3)
Flare 1	55853.5–55854.5	14.86 ± 0.89	1.97 ± 0.04
Flare 2	55872–55874	8.39 ± 0.44	2.19 ± 0.04

(1) Dates of the γ -ray flux maxima in the daily-binned light curve; (2) photon fluxes measured at the flux maxima in the units of $[10^{-6} \text{ ph cm}^{-2} \text{ s}^{-1}]$, averaged over the specified time intervals; (3) the corresponding photon indices. All the values are taken from Saito et al. (2013).

spectral slopes below and above the break, respectively, often change significantly on the timescales of less than a day (Abdo et al. 2009, 2011; Tanaka et al. 2011; Stern & Poutanen 2011; Rani et al. 2013). This indicates that the γ -ray data integrated over longer periods of time, which are typically utilized in the blazar SED modeling, should be considered as a superposition of different spectra produced at different stages of the jet evolution, and as such may hardly be used for any exact spectral diagnosis. Of course, in the overwhelming majority of cases long integration LAT exposures times are unavoidable, due to a limited photon statistics. Still, the caution should be kept in mind.

This situation has motivated us to attempt a detailed, *time-dependent*, and fully *self-consistent* modeling of the spectral evolution of bright γ -ray flares in FSRQs, for which the time profiles can be resolved and the spectra can be constrained on the hourly timescales. In particular, in this paper we present the extensive modeling of the extremely bright γ -ray flares in PKS 1510–089, which were analyzed before by Saito et al. (2013, see also Brown 2013 and Foschini et al. 2013). This allows us to put uniquely robust (though still model-dependent, to some extent) constraints on the structure and the location of the flaring emission zone in the source, as discussed further below.

Throughout the paper we assume the Λ CDM cosmology with $\Omega_\Lambda = 0.73$, $\Omega_M = 0.27$, and $H_0 = 71 \text{ km s}^{-1} \text{ Mpc}^{-1}$, so that the redshift of PKS 1510–089, $z = 0.361$, corresponds to the luminosity distance of $d_L \simeq 1.91$ Gpc.

2. SELECTION OF THE *FERMI*-LAT DATA

The *Fermi*-LAT provides the most complete and sensitive coverage of the γ -ray sky up to date. Since 2008 it surveys the entire sky every three hours within the photon energy range 20 MeV – 300 GeV, so that each astrophysical γ -ray source — majority of which are blazars (Nolan et al. 2012) — is exposed for about 30 min during one scan. Due to the limited photon statistics, the selection of the *Fermi*-LAT data for this work has to focus inevitably on the flaring states of the brightest FSRQs, for which meaningful spectral analysis could be performed with the minimum LAT time resolution. We further restrict our modeling to the well-resolved γ -ray flares of PKS 1510–089 which occurred in 2011, as summarized in Table 1 following the analysis of Saito et al. (2013). These two flares constitute the best known examples of the prominent, isolated, and coherent events, unlike the majority of the observed blazar flux enhancements which

TABLE 2
MODEL PARAMETERS OF THE “FREE-EXPANDING JET” FIT TO THE γ -RAY FLARES OF PKS 1510–089.

Model parameter	Flare 1	Flare 2	reference
Minimum electron Lorentz factor, γ_{\min}	1		Barnacka et al. (2014)
Break electron Lorentz factor, γ_{br}	900		”
Maximum electron Lorentz factor, γ_{\max}	1×10^5		”
Low-energy electron injection index, p	1.2		”
High-energy electron injection index, q	3.4		”
Bulk Lorentz factor of the emitting shell, Γ	22		”
Jet opening angle, θ_{jet}	2.6 deg		”
Jet viewing angle, θ_{obs}	2.6 deg		”
Jet magnetic field intensity at 10^{18} cm, B_0	0.75 G		”
Characteristic scale of the BLR, R_{BLR}	0.12×10^{18} cm		”
Central energy density of the BLR photon field, u_{BLR}	0.06 erg cm^{-3}		”
Characteristic energy of the BLR photons, $h\nu_{\text{BLR}}$	10 eV		”
Characteristic scale of the HDT, R_{HDT}	1.94×10^{18} cm		”
Central energy density of the HDT photon field, u_{HDT}	$5 \times 10^{-4} \text{ erg cm}^{-3}$		”
Characteristic energy of the HDT photons, $h\nu_{\text{HDT}}$	0.15 eV		”
Normalization of the electron injection function, K_e	$1.6 \times 10^{47} \text{ s}^{-1}$	$0.6 \times 10^{47} \text{ s}^{-1}$	this work, § 4.1
Distance where the injection starts, R_{start}	0.7×10^{18} cm	2.3×10^{18} cm	”
Distance where the injection terminates, R_{stop}	0.9×10^{18} cm	3.4×10^{18} cm	”
Distance where the simulation stops, R_{end}	2.3×10^{18} cm	6.9×10^{18} cm	”

seem rather like a superposition of distinct (though possibly related) but just unresolved sub-flaring/flickering.

The question remains if the minimum (orbital) 3-hour binning of the LAT data is sufficiently short for resolving the PKS 1510-089 flares properly. We note in this context that the stochastic modeling of the LAT light curves for the brightest blazars by Sobolewska et al. (2014) revealed some hints for sub-hour variability timescales in only four sources, *not* including PKS 1510–089. These characteristic variability timescales regarded the features of the γ -ray power spectral density functions, and not the flux doubling timescales studied by Saito et al. (2013) or Brown (2013). Taking therefore into account that the rising and decaying phases of the two flares selected for our analysis are very well defined, with no sub-structure appearing even when studied with the shortest binning (Saito et al. 2013), we conclude that one can indeed consider a single emitting component to be responsible for the observed flux evolution during the targeted activity epochs of the source, and hence that a meaningful time-dependent modeling can be performed in the framework of a given jet model. The issue of sub-orbital blazar variability in the LAT data will be analyzed in detail in the forthcoming paper Saito et al. (2015, in prep.).

3. THE MODEL

We simulate the time evolution of the observed source spectrum during the selected flaring events utilizing the BLAZAR code, which was developed by Moderski et al. (2003, 2005) based on the widely anticipated scenario of internal shocks formed by colliding blobs of the jet plasma (e.g., Sikora et al. 1994; Spada et al. 2001; Böttcher & Dermer 2010; Mimica & Aloy 2012; Rueda-Becerril et al. 2014, see § 5 for the detailed model description). The model can be however applied to a more general situation as well, since it only approximates the flaring emission region with a uniform and expanding shell of the emitting plasma moving along the outflow, and follows self-consistently the evolution of the radiating particles injected into the shell, but does not involve any particular assumption on the exact particle acceler-

ation process involved.

More specifically, in the model the electron injection is assumed to take place at a constant rate with a fixed injection spectrum for a given instance of time when the shell moves from R_{start} to R_{stop} , and to be negligible otherwise. The time evolution of the injected electron energy distribution is calculated in the emitting plasma rest frame (denoted below by primes) following the standard kinetic equation

$$\frac{\partial N_\gamma}{\partial t'} = -\frac{\partial}{\partial \gamma} \left(N_\gamma \frac{d\gamma}{dt'} \right) + Q_\gamma, \quad (1)$$

where N_γ is the comoving number density of electrons with Lorentz factor γ , and Q_γ is the electron injection function. In this paper we do not prime the electron Lorentz factors γ , noting instead that these always refer to the emitting plasma rest frame. Radiative energy losses due to the synchrotron emission and the inverse-Compton radiation, as well as the adiabatic losses due to the radial expansion of the emitting shell, are all taken into account self-consistently in the $d\gamma/dt'$ term. For those, the jet magnetic field is assumed to decrease along the outflow as $B'(R) \propto R^{-1}$, corresponding to the case of the conserved magnetic energy flux with the dominant toroidal component. The energy densities of the external target photon fields for the inverse-Compton scattering, namely of the BLR and of the hot dusty torus (HDT), are assumed to be isotropic in the observer frame and to scale with the distance from the core as

$$u'_{\text{ext}}(R) = \frac{\Gamma^2 L_{\text{ext}}}{4\pi c R_{\text{ext}}^2} \frac{1}{1 + (R/R_{\text{ext}})^2}, \quad (2)$$

where R_{ext} is the characteristic radius and L_{ext} represents the total luminosity of a given field (see Sikora et al. 2009)⁶. We note that the BLAZAR code offers the correct treatment of the quantum (Klein-Nishina) effects when

⁶ See in this context Janiak et al. (2015), Appendix A1 therein, for the alternative scaling of the BLR energy density with the distance from the central engine.

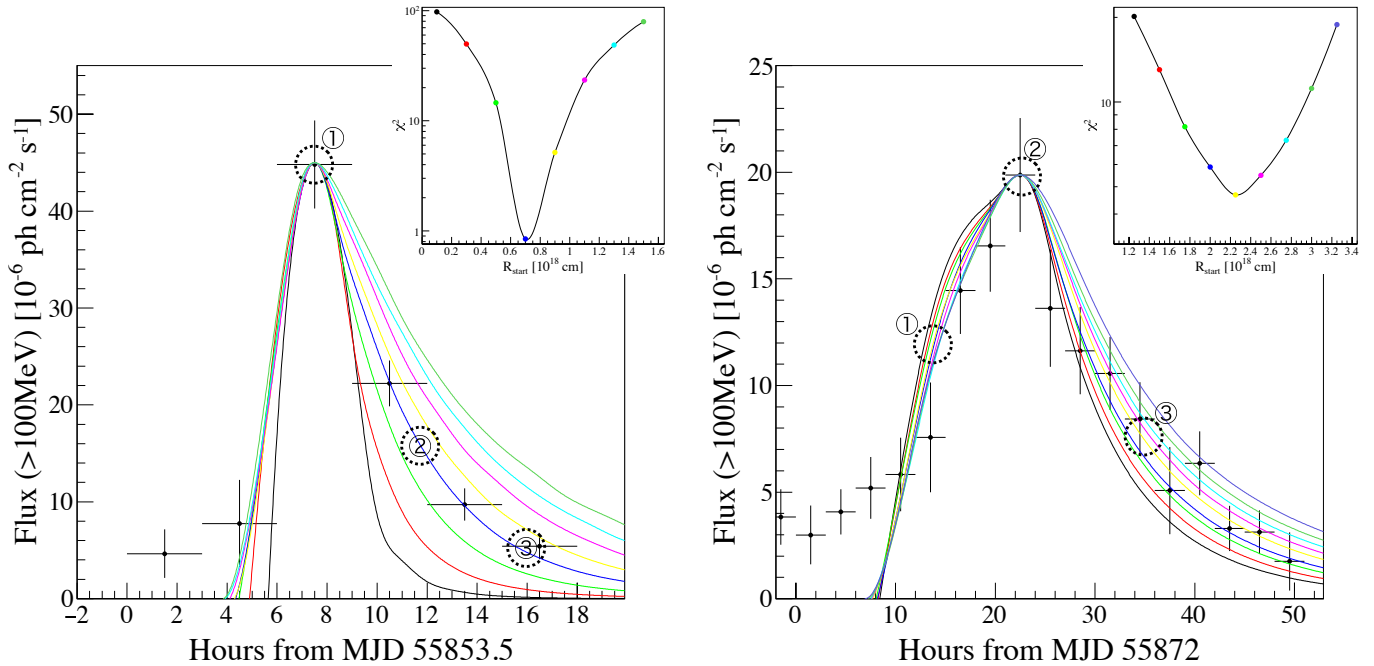


FIG. 1.— Simulated profiles of the analyzed Flare1 and Flare2 in PKS 1510–089 within the 0.1–300 GeV range (left and right panels, respectively), superposed on the 3-hour binned LAT light curve of the source taken from Saito et al. (2013). Simulations denoted in the figure by various color curves were performed for different locations of the emitting region along the free-expanding outflow, as explained in the text (see § 4.1). The χ^2 values for the corresponding model fits to the decaying phases of the flares are inserted as small figures in the panels. The resulting best-fit parameters are given in Table 2. The broad-band emission spectra presented in Figure 3 below coincide with the instants marked as “1”, “2”, and “3” in the panels. We note the long-term averaged flux level of the source is 2.7×10^{-7} ph cm $^{-2}$ s $^{-1}$ above 100 MeV, according to the *Fermi*-LAT 3FGL catalog (Acero et al. 2015).

calculating the inverse-Compton emission (see the discussion in Moderski et al. 2005).

We parametrize the electron injection spectrum by a broken power-law

$$Q_\gamma = K_e \gamma^{-p} \left[1 + \left(\frac{\gamma}{\gamma_{\text{br}}} \right)^4 \right]^{\frac{1}{4}(p-q)}, \quad (3)$$

where K_e is the normalization parameter, p and q are the low- and high-energy injection indices, respectively, and γ_{br} is the critical/break electron Lorentz factor. The injection function is defined within the range of $\gamma_{\text{min}} \leq \gamma \leq \gamma_{\text{max}}$.

After simulating the evolution of the electron energy distribution while the shell propagates along the jet based on the equation of balance (1), the observed SED at a given instance of time is calculated by integrating radiative contributions from all the cells located at different radial distances within the shell over the viewing angle θ_{obs} . The corresponding γ -ray light curve is obtained by extracting the γ -ray flux at each step of the simulation (see Moderski et al. 2003, for the full description).

4. TIME-DEPENDENT MODELING

Several input parameters for the time-dependent simulations of the analyzed flares were selected based on the recent broad-band fitting of the PKS 1510–089 spectrum during the 2009 flaring state by Barnacka et al. (2014). The main characteristics of the external photon fields (BLR and HDT, in particular) were fixed following the detailed studies of the accretion disk emission in the

source by Nalewajko et al. (2012a). All of these are summarized in Table 2. The jet opening and viewing angles were at first assumed as $\theta_{\text{jet}} = \theta_{\text{obs}} = 1/\Gamma$, where Γ is the bulk Lorentz factor of a moving shell (§ 4.1); in the following steps of the modeling we also considered smaller values of θ_{jet} , in accord with the most recent results of the high-resolution radio observations of blazar jets (see § 4.2 and references therein).

4.1. “Free-Expanding Jet” Model

The critical distances along the outflow marking the onset and the termination of the electron injection, R_{start} and R_{stop} , respectively, i.e. the two crucial free parameters of our modeling, were constrained under the condition of a free-expanding outflow $\theta_{\text{jet}} = \theta_{\text{obs}} = 1/\Gamma = 2.6$ deg in the following way. First, the interval $\Delta R = R_{\text{stop}} - R_{\text{start}}$ was determined from the observed rising time of the flare τ_{fl} using the general relation $\Delta R = c \Gamma \delta \tau_{\text{fl}} / (1+z)$. Next, for a given fixed ΔR we varied R_{start} and R_{stop} together with the normalization of the injection function K_e , evaluated the resulting γ -ray fluxes within the 0.1–300 GeV range for each set of the model parameters (up to the distance $R_{\text{end}} > R_{\text{stop}}$), and fitted the observed *Fermi*-LAT light curves with the simulated profiles. The final values of the free parameters were then chosen based on the χ^2 of the model fits to the decaying phases of the flares. The results of the simulations are presented in Figure 1.

In the case of the Flare 1, the best model fit to the data returns $R_{\text{start}} = 0.7 \times 10^{18}$ cm and $R_{\text{stop}} = 0.9 \times 10^{18}$ cm, with the γ -ray emission settling down around $R_{\text{end}} = 2.3 \times 10^{18}$ cm with the uncertainty of 0.1×10^{18} cm. Sim-

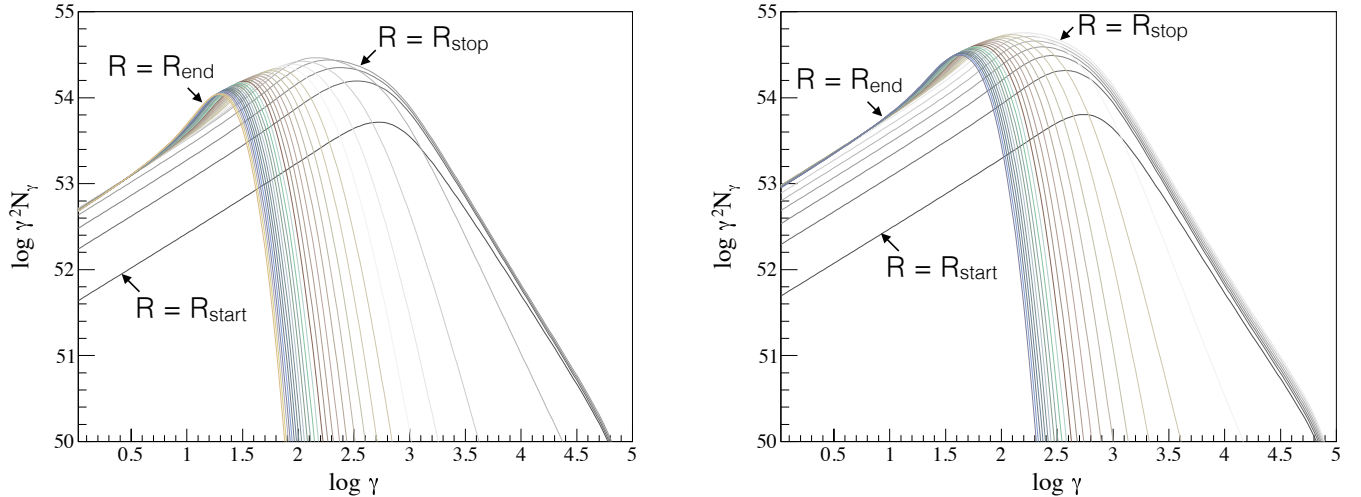


FIG. 2.— The simulated evolution of the electron energy distribution as the emitting shell propagates along the free-expanding jet during the analyzed Flare1 and Flare2 (left and right panels, respectively), corresponding to the sets of the model parameters given in Table 2 .

ilarly, for the Flare2 we obtain $R_{\text{start}} = 2.3 \times 10^{18}$ cm, $R_{\text{stop}} = 3.4 \times 10^{18}$ cm, and $R_{\text{end}} = 6.9 \times 10^{18}$ cm, with the uncertainty of 0.3×10^{18} cm. Overall, the studied γ -ray flare light curves can be fitted reasonably well under all the model assumptions specified above, although the well-resolved rising profiles of the flares (especially of the Flare2) seem to suggest a more complex time-dependence of the electron injection function at the very beginning of the acceleration process.

The simulations performed allow us to propagate the evolution of the electron and the broad-band emission spectra during the analyzed epochs (though it should be noted at the same time that the photon statistics of the available *Fermi*-LAT data precludes us from any precise characterization of the γ -ray spectral changes in the source in three-hour bins). Figure 2 presents the results of the simulations regarding the evolution of the electron energy distribution as the emitting shell moves along the free-expanding outflow. As shown, until the injection stops, the number of the injected relativistic electrons grows. After the injection terminates, higher energy electrons cool very rapidly, so that the break energy in the evolved electron spectrum decreases with time, and the high-energy continuum steepens. At the later stages of the evolution ($R \sim R_{\text{end}}$), a moderate pile-up can be noted around electron energies $\gamma \lesssim 100$. The reason for this pile-up is however not the Klein-Nishina suppression of the inverse-Compton scattering efficiency (see Dermer & Atoyan 2002; Moderski et al. 2005), but instead the fact that at such late evolutionary stages the low-energy segment of the electron distribution, characterized by the injection spectral index $p < 2$, becomes subjected to the efficient radiative cooling $d\gamma/dt' \propto \gamma^2$ (see in this context Kardashev 1962). We also note that no pronounced spectral hardening due to the Klein-Nishina effects at higher electron energies is seen in our simulations, because the flare is produced effectively outside the BLR and the injected high-energy segment of the electron continuum is steep (c.f. Cerruti et al. 2013); we have however confirmed that cooled electron spectrum becomes softer above electron Lorentz factors $\gamma \sim 10^3$ when Klein-

Nishina suppression is ignored.

The corresponding evolution of the broad-band jet flaring spectra is shown in Figure 3, including the synchrotron, synchrotron self-Compton (SSC), and the two “external-Compton” (EC/BLR and EC/HDT) emission components. As shown, in the case of the Flare1, the EC/HDT component dominates the production of the high-energy continuum from the observed hard X-ray up to ~ 100 MeV photon energies; the soft X-ray range is dominated by the SSC emission, the GeV range by the EC/BLR process, and in the TeV range the two EC components becomes again comparable. In the case of the Flare2, on the other hand, the SSC and EC/BLR processes are in general much less relevant, as expected taking into account the larger size and distance of the emitting region involved in the production of this flare.

Unfortunately, no simultaneous broad-band data are available for the two flares analyzed here. Saito et al. (2013) reported that the photon indices within the LAT range during the flares were approximately $\simeq 2.0$, which is roughly consistent with the spectra simulated in this work given the large uncertainty range. For a reference, in Figure 3 we included the archival spectral datapoints corresponding to the March 2009 flare of PKS 1510–089 from Barnacka et al. (2014).

Let us finally comment on the asymmetric profiles of the modeled flux enhancements. The standard view on this issue is that longer decay phases of blazar flares when compared with the flux rising phases reflect longer radiative cooling timescales when compared with extremely rapid, almost instantaneous particle acceleration timescales, or even with the short but finite injection intervals controlled by the macroscopic (shock dynamical) timescales (as anticipated in our work). However, radiative cooling timescales in PKS 1510–089 jet at sub-pc/pc scales are typically expected to be much shorter than the observed decay timescales of the 2011 flares (see the discussion in Saito et al. 2013).

And indeed, our simulations reveal that the dominant factor shaping the flux decay profiles is not the radiative cooling of the high-energy particles, but instead a

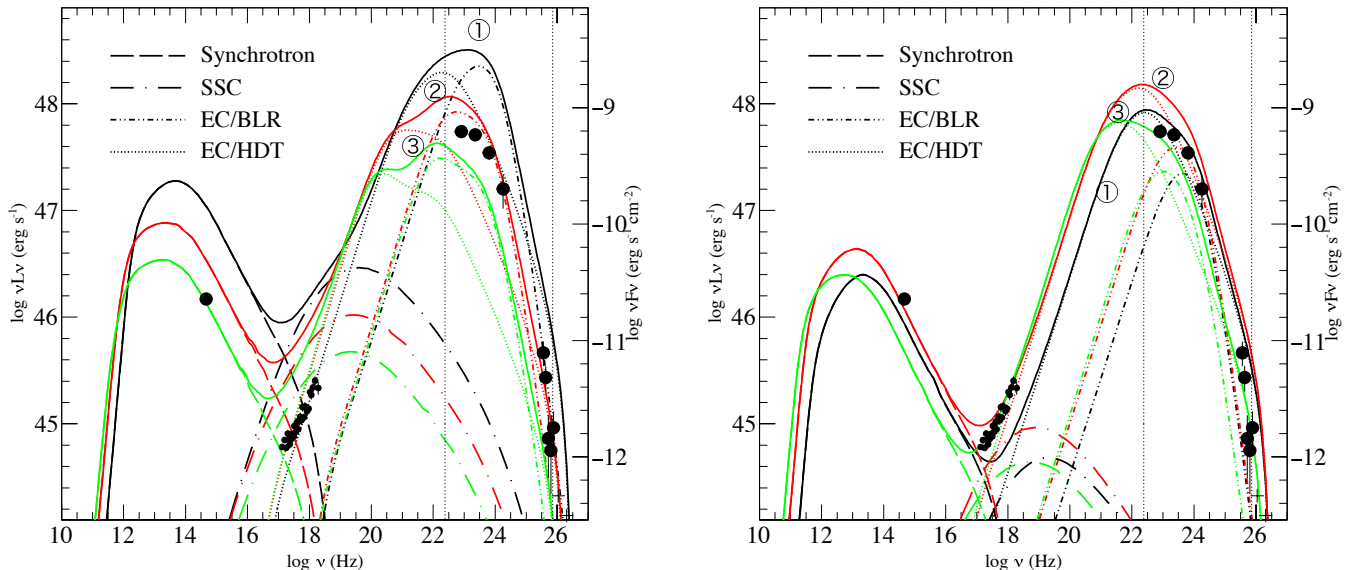


FIG. 3.— The simulated time evolution of the broad-band SEDs of PKS 1510–089 during the analyzed Flare 1 and Flare 2 (left and right panels, respectively). The spectra were extracted at the instants marked as “1”, “2”, and “3” in Figure 1 (black, red, and green curves, respectively). Vertical dashed lines indicate the energy range of 100 MeV – 300 GeV. For a reference, in the plots we include also the archival spectral datapoints corresponding to the March 2009 flare of the source from Barnacka et al. (2014). Calendar dates are October 19.5–20.5, 2011 for Flare 1 and November 7–9, 2011 for Flare 2.

gradient of the Doppler factor across the emitting shells of the jet plasma. Namely, for the model parameters considered above in this section, the emitting shells are relatively thin but instead considerably extended in the radial direction (see § 5), so that different parts of the shells are observed at different viewing angles. As a result, emission produced within the parts characterized by the largest inclinations arrive to the observer with a significant delay when compared with the emission output of the parts located at smaller viewing angles.

This effect is visualized in Figure 4, where we present the simulated profiles of the Flare 1 corresponding to the different values of the jet opening angle (equal by assumption to the jet viewing angle), and all the other model parameters fixed as before except for the adjusted electron normalization. As shown, with the decreasing jet opening angle the variance of the Doppler factor across the emitting shell becomes smaller, and as a result the flare’s asymmetry decreases. Only for the dramatically small $\theta_{\text{jet}} = \theta_{\text{obs}} = 0.3$ deg the simulated decaying timescale becomes comparable to the radiative cooling timescale of the γ -ray emitting electrons.

4.2. “Collimated Jet” Model

Due to the causality requirement, for a free-expanding jet one has $\Gamma \theta_{\text{jet}} \simeq 1$ at most, the condition which is often anticipated in blazar modeling. However, several recent radio studies of relativistic jets in blazar sources imply highly collimated outflows on milli-arcsec scales, with small opening angles $\Gamma \theta_{\text{jet}} \simeq 0.1$ (e.g., Clausen-Brown et al. 2013; Jorstad et al. 2005; Zdziarski et al. 2015). In order to investigate such a possibility in more detail, we repeated simulations of the selected flares in the source assuming different values of $0.1 \leq \Gamma \theta_{\text{jet}} \leq 1$ (for the fixed $\Gamma = 22$). We again imposed the condition $\theta_{\text{obs}} = \theta_{\text{jet}}$, so that the relativistic beaming is maximized; this requirement is necessary, since in the case

of a misaligned PKS 1510–089 jet (i.e., for $\theta_{\text{obs}} > \theta_{\text{jet}}$), unrealistically large electron injection is needed in order to produce the observed γ -ray flux enhancements.

The resulting best-fit positions of the onset of the γ -ray emitting regions for different values of θ_{jet} , and the corresponding normalizations of the electron injection, are presented in Figure 5. For both flares considered, the location of the emission zone increases further away from the SMBH as the jet opening angle decreases. This dependence may be understood by considering the effect of the Doppler factor gradient discussed in the previous section. In particular, for smaller and smaller θ_{jet} , the Doppler factor variance across the emitting shell decreases; as a result, the emission region have to be placed further and further away from the jet base so that the increased electron cooling timescales can support the extended decay phases of the flares (note that at larger distances from the core the energy densities of the BLR and HDT photon fields decrease, and hence the corresponding radiative cooling timescales increase).

In the case of the highly collimated jet with particularly small $\theta_{\text{jet}} \simeq 0.26$ deg, the best-fit position of the emission zone turns out as $R_{\text{start}} \simeq 4.3 \times 10^{18}$ cm for the Flare 1, and $R_{\text{start}} \simeq 8.1 \times 10^{18}$ cm for the Flare 2. Together with the simulation results presented in the previous section, this indicates therefore a relatively narrow range allowed for the production of the observed γ -ray flares in PKS 1510–089, namely 10^{19} cm $\geq R_{\text{start}} \geq 10^{18}$ cm for the jet opening angle $0.1 \leq \Gamma \theta_{\text{jet}} \leq 1$. At the same time, the required amount of the electron injection for producing the observed γ -ray luminosity may be substantially smaller for a well-collimated outflow (see the lower panels in Figure 5). This means that in the case of a jet with $\Gamma \theta_{\text{jet}} < 1$ it is “easier” to produce huge γ -ray outbursts with the total released radiative power of the order of the accretion disk luminosity, while somewhat extreme conditions are needed for such a maximum effi-

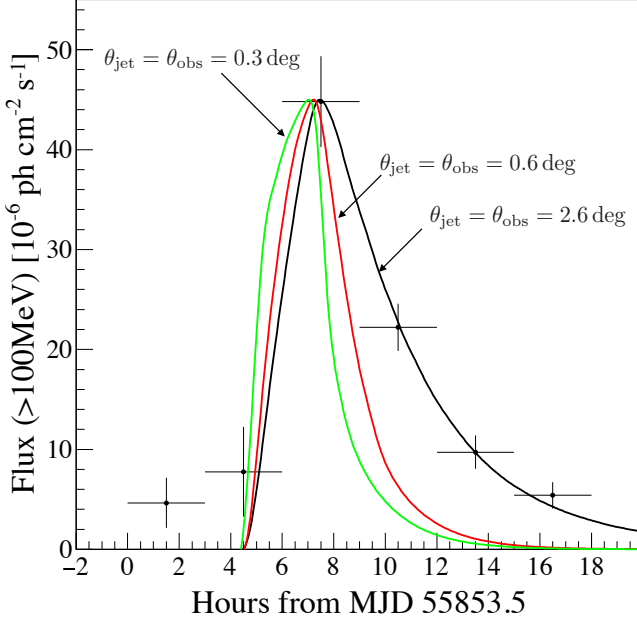


FIG. 4.— Simulated profiles of the Flare 1 assuming different values of the jet opening angle (and other parameters as given in Table 2 except for the adjusted electron normalization), which illustrate the effect of the Doppler factor gradient across the emitting shell in the PKS 1510–089 jet (see § 4.1 for the discussion).

ciency in the case of a standard, free-expanding jet with $\Gamma_{\text{jet}} \simeq 1$ (see the discussion in the following section).

5. DISCUSSION

In the framework of the internal shock scenario, a collision of two plasma blobs characterized by different bulk Lorentz factors $\Gamma_1 \equiv (1 - \beta_1^2)^{-1/2}$ and $\Gamma_2 \equiv (1 - \beta_2^2)^{-1/2}$ produces the double-shock shock structure propagating within the merged portion of the jet matter. It is assumed that the electrons are accelerated at the shock fronts, and are injected with a given energy spectrum into the downstream region where they cool radiatively and adiabatically. The resulting shock velocity can be found under the specific assumptions on the dynamics of the colliding plasmoids. In particular, if the colliding portions of the jet flow differ only in bulk velocities, and the jet magnetic field is negligible dynamically, as assumed in this paper, the downstream (emitting) plasma is characterized by the bulk Lorentz factor $\Gamma \equiv (1 - \beta^2)^{-1/2} \sim \sqrt{\Gamma_1 \Gamma_2}$ as long as $\Gamma_2 > \Gamma_1 \gg 1$ (e.g., Stawarz et al. 2004; Moderski et al. 2004). In the upstream region rest frame (denoted below by double-primes), moving with the velocity β_1 relative to the observer, the bulk Lorentz factor of the shock is

$$\Gamma''_{\text{sh}} = \sqrt{\frac{(\Gamma'' + 1)(4\Gamma'' - 1)^2}{8\Gamma'' + 10}}, \quad (4)$$

where

$$\beta'' = \frac{\beta - \beta_1}{1 - \beta\beta_1}. \quad (5)$$

This implies that the resulting shock velocity in the downstream region rest frame (denoted in this paper by

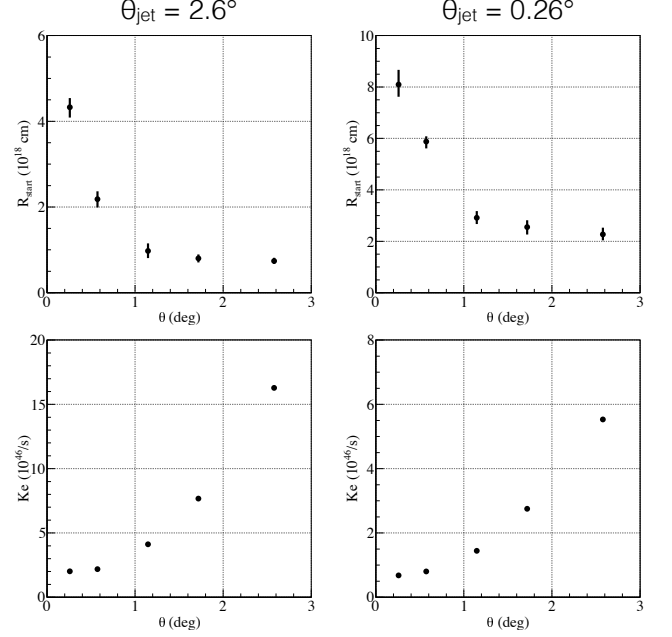


FIG. 5.— The best-fit location of the onset of the flaring zone (upper panels) and the corresponding normalization of the electron injection function (lower panels) for the Flare 1 and Flare 2 (left and right panels, respectively), as functions of the jet opening angle $\theta_{\text{jet}} = \theta_{\text{obs}}$ (see § 4.2 for the discussion).

primes),

$$\beta'_{\text{sh}} = \frac{\beta''_{\text{sh}} - \beta''}{1 - \beta''_{\text{sh}} \beta''}, \quad (6)$$

saturates at the approximately constant value of $\beta'_{\text{sh}} \sim 0.1$ (Stawarz et al. 2004).

The observed rising timescale of a flare, τ_{fl} , may be identified with the time interval τ_{inj} when active shocks propagating through the outflow inject freshly accelerated electrons into the downstream region (which is a moving portion of the jet matter). Hence, the shell width in the emitting region rest frame is

$$\ell'_{\text{sh}} = 2c\beta'_{\text{sh}}\tau'_{\text{inj}} \simeq 2c\beta'_{\text{sh}}\delta\tau_{\text{fl}}. \quad (7)$$

On the other hand, the transverse extension of the emitting region can be estimated simply as

$$r' = r \simeq R_{\text{stop}}\theta_{\text{jet}}. \quad (8)$$

In the case of the Flare 1, for which the observed rising timescale is of the order of three hours, one has for example $\ell'_{\text{sh}} \sim 1.5 \times 10^{15}$ cm and $r' \simeq 4 \times 10^{16}$ cm under the condition of a free-expanding jet with $\theta_{\text{jet}} = \theta_{\text{obs}} = 1/\Gamma \simeq 2.6$ deg; the emerging ratio $\ell'_{\text{sh}}/r' \sim 0.035$ implies therefore an extremely thin shell of the emitting plasma, even at the final stages of the shock evolution. Note, however, that in the observer frame an almost spherical apparent shape would be measured, namely $\ell_{\text{sh}}/r = \delta\ell'_{\text{sh}}/r' \sim 0.8$. The intrinsic aspect ratio of the emitting region increases, on the other hand, in the case of a well-collimated jet. In particular, with the jet opening and viewing angles $\theta_{\text{jet}} \simeq \theta_{\text{obs}} \simeq 0.26$ deg, the downstream region linear scale reads as $\ell'_{\text{sh}} \sim 3 \times 10^{15}$ cm, and the emitting region radius becomes $r' \simeq 4 \times 10^{15}$ cm, leading to $\ell'_{\text{sh}}/r' \sim 0.7$, or $\ell_{\text{sh}}/r \sim 30$ in the observer frame. In the case of the Flare 2, characterized by the observed flux rising

timescale of the order of 12 hours, the analogous values read as $\ell'_{\text{sh}} \sim 6 \times 10^{15}$ cm and $r' \simeq 1.5 \times 10^{17}$ cm for $\theta_{\text{jet}} \simeq 2.6$ deg, or $\ell'_{\text{sh}} \sim 10^{16}$ cm and $r' \simeq 1.5 \times 10^{16}$ cm for $\theta_{\text{jet}} \simeq 0.26$ deg, so that the corresponding aspect ratio are basically the same as for the Flare 1.

The total number of electrons injected into the emitting shell during the shock activity period,

$$\mathcal{N}_e = \int dt' \int d\gamma Q_\gamma = \tau'_{\text{inj}} \times \int d\gamma Q_\gamma, \quad (9)$$

together with the electron mean energy,

$$\langle \gamma_{\text{inj}} \rangle = \frac{\int d\gamma \gamma Q_\gamma}{\int d\gamma Q_\gamma}, \quad (10)$$

gives the jet comoving energy density of the radiating electrons

$$u'_e = \frac{\langle \gamma_{\text{inj}} \rangle m_e c^2 \mathcal{N}_e}{\pi r'^2 \ell'_{\text{sh}}}. \quad (11)$$

Hence, the electron kinetic flux (including also the power dissipated radiatively during the flare) reads as

$$\begin{aligned} L_e &= \pi r'^2 c \beta \Gamma^2 u'_e \\ &= \frac{1}{2} \beta \Gamma^2 \beta'^{-1}_{\text{sh}} m_e c^2 \times \int d\gamma \gamma Q_\gamma \end{aligned} \quad (12)$$

(see equation 7). With the best-fit parameters of the free-expanding jet model (see Table 2), one obtains therefore $L_e \simeq 1.3 \times 10^{47}$ erg s⁻¹ for the Flare 1, and $L_e \simeq 0.5 \times 10^{47}$ erg s⁻¹ for the Flare 2.

With the aforementioned model parameters, the electron mean energy reads as $\langle \gamma_{\text{inj}} \rangle \simeq 110$. In the framework of the anticipated internal shock scenario, assuming in addition that the upstream jet plasma is cold (meaning at most trans-relativistic energies of plasma particles), this value excludes a pure electron-positron content of the PKS 1510–089 jet. That is because in the case of a pure pair plasma, the energy conservation $\langle \gamma_{\text{inj}} \rangle \Gamma \mathcal{N}_e m_e c^2 \simeq \frac{1}{2} \Gamma_2 \mathcal{N}_e m_e c^2$ would then imply unrealistically high bulk Lorentz factor of the faster shell, namely $\Gamma_2 \sim 5000$ (for the the downstream bulk Lorentz factor $\Gamma = 22$). Hence, self-consistency of the modeling presented in this paper requires protons to dominate the plasma inertia.

Let us therefore assume that the colliding shells with total energies E_1 and E_2 are initially dominated by cold protons with the total number \mathcal{N}_p . Under the $\Gamma_2 > \Gamma_1 \gg 1$ assumption specified previously, one can derive the efficiency of the energy dissipation after the shells' collision as

$$\eta_{\text{diss}} = \frac{E_{\text{diss}}}{E_1 + E_2} \simeq \frac{(\Gamma_2/\Gamma - 1)^2}{(\Gamma_2/\Gamma)^2 + 1}. \quad (13)$$

Quantifying next the energy dissipated per proton in the $m_p c^2$ units as

$$\kappa \equiv \frac{E'_{\text{diss}}}{\mathcal{N}_p m_p c^2}, \quad (14)$$

and keeping in mind that $E_1 = \frac{1}{2} \Gamma_1 \mathcal{N}_p m_p c^2$, $E_2 = \frac{1}{2} \Gamma_2 \mathcal{N}_p m_p c^2$, and $E'_{\text{diss}} = E_{\text{diss}}/\Gamma$, one can find

$$\kappa \simeq \frac{1}{2} \frac{(\Gamma_2/\Gamma - 1)^2}{\Gamma_2/\Gamma}. \quad (15)$$

And since $\langle \gamma_{\text{inj}} \rangle \mathcal{N}_e m_e c^2 = \eta_e E'_{\text{diss}}$, where η_e is the efficiency of the energy transfer to relativistic electrons at the shock front, the composition of the jet can be finally estimated as

$$\frac{\mathcal{N}_e}{\mathcal{N}_p} \simeq \eta_e \kappa \frac{m_p/m_e}{\langle \gamma_{\text{inj}} \rangle} \quad (16)$$

(see, e.g., Moderski et al. 2004). The typically considered value of $\eta_e \simeq 0.5$ and a pure electron-proton jet composition $\mathcal{N}_e/\mathcal{N}_p \simeq 1$ imply therefore $\Gamma_2 \simeq 35$ with the corresponding $\eta_{\text{diss}} \simeq 0.1$. Any larger amount of electron-positron pairs in the jet would increase both the bulk Lorentz factor of the faster shell (for the given Γ), and the overall energy dissipation efficiency; for example, $\mathcal{N}_e/\mathcal{N}_p \simeq 3$ (meaning the pair content $\mathcal{N}_{e^+}/\mathcal{N}_{e^-} \simeq 0.5$) would require a still reasonable value of $\Gamma_2 \simeq 50$, with the corresponding $\eta_{\text{diss}} \simeq 0.25$. Note in this context that the outflows remains dominated dynamically by protons,

$$\frac{L_p}{L_e} = \frac{1}{\mathcal{N}_e/\mathcal{N}_p} \frac{m_p/m_e}{\langle \gamma_{\text{inj}} \rangle} > 1 \quad (17)$$

as long as $\mathcal{N}_e/\mathcal{N}_p < 10$. In particular, with $\mathcal{N}_e/\mathcal{N}_p \simeq 1 - 3$ adopted hereafter, one has $L_p/L_e \sim 10$.

The total luminosity of the accretion disk in PKS 1510–089 was estimated by Nalewajko et al. (2012a) as $L_{\text{disk}} \simeq 5 \times 10^{45}$ erg s⁻¹, meaning the accretion power in the system of the order of $L_{\text{acc}} \sim 10^{47}$ erg s⁻¹ (for the assumed the standard, 10% radiative efficiency factor). The model parameters evaluated above under the $\Gamma \theta_{\text{jet}} \simeq 1$ condition, imply therefore an extreme efficiency of the jet production, with the total jet kinetic power $L_j \simeq L_p \sim 10 L_{\text{acc}}$. In the case of a highly collimated jet, this efficiency may be decreased quite significantly (see Figure 5). On the other hand, the jet magnetic field within the blazar emission zone, which is rather weak already in the free-expanding jet case, becomes even less relevant dynamically with the decreasing product $\Gamma \theta_{\text{jet}}$. In particular, with $\theta_{\text{jet}} \simeq 2.6$ deg, the ratio of the electron kinetic energy and Poynting fluxes,

$$\frac{L_e}{L_B} = \frac{2 m_e c^2}{c \beta'^2_{\text{sh}}} \times \frac{\int d\gamma \gamma Q_\gamma}{[R \theta_{\text{jet}} B'(R)]^2}, \quad (18)$$

reads as $L_e/L_B \sim 60$ and ~ 20 for the Flare 1 and the Flare 2, respectively. Assuming instead $\theta_{\text{jet}} \simeq 0.26$ deg, but keeping a comparably large Compton dominance in the source (i.e., the ratio of the high-energy and synchrotron peak luminosities $\sim 10 - 100$), we obtain worrisomely small jet magnetization of $L_e/L_B \gtrsim 100$.

It is interesting to note in this context that the model fit to the *average/quiescence* broad-band spectrum of PKS 1510–089 using the BLAZAR code, presented in Kataoka et al. (2008), indicates $L_p \simeq 2 \times 10^{46}$ erg s⁻¹ and $L_e \simeq L_B \simeq 0.6 \times 10^{46}$ erg s⁻¹. This, together with the results of our simulations, may suggest that while during the extended source quiescence the outflow is in equipartition between the relativistic electron and magnetic field energy fluxes, with the total jet kinetic luminosity dominated only slightly by cold protons and constituting only some smaller fraction of the available accretion power ($L_{\text{acc}} \sim 10 L_p$ with $L_e \sim L_B \sim 0.3 L_p$), dramatic though relatively rare flaring events consist of an excess energy flux carried out predominantly by the

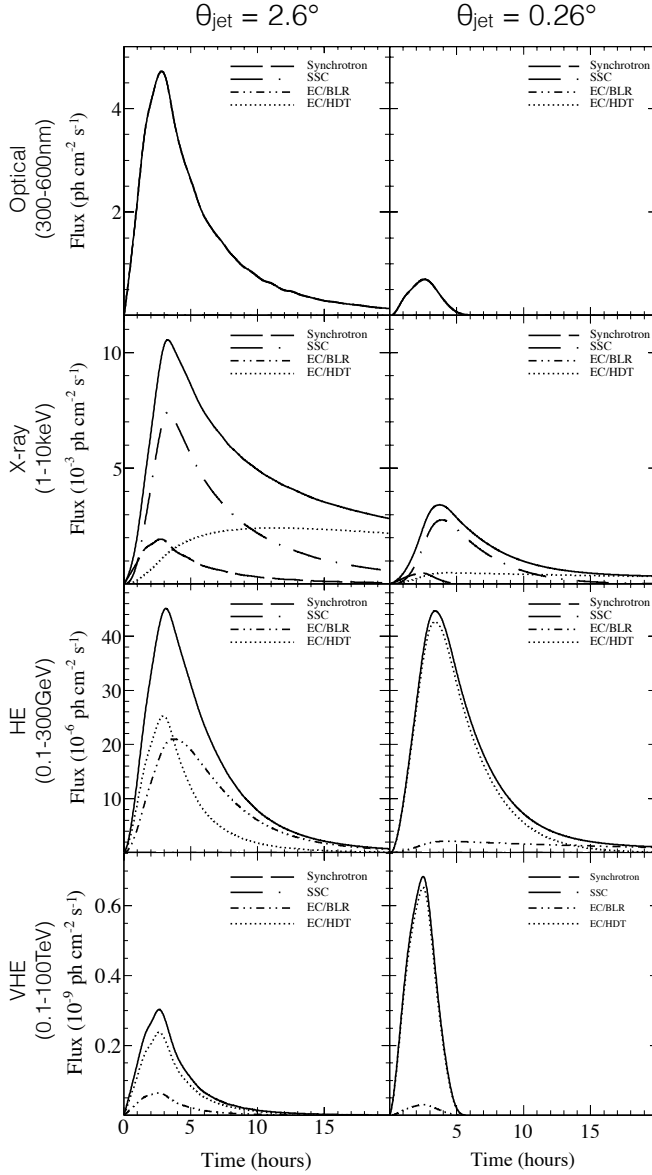


FIG. 6.— Simulated light curves corresponding to the Flare 1 in optical, X-rays, HE γ -rays, and VHE γ -rays (top to bottom, respectively), for the cases of a free expanding conical jet ($\theta_{\text{jet}} = \theta_{\text{obs}} = 1/\Gamma$, left panels), and a collimated jet (with $\theta_{\text{jet}} = \theta_{\text{obs}} = 0.1/\Gamma$, right panels). The location of the emission zone and the normalization of the electron injection are fixed at the best-fit values for the HE γ -ray flares (see Figure 4). Various emission components are denoted by different styles of the curves (dashed, dot-dashed, dot-dot-dashed, and dotted) for the synchrotron, SSC, EC/BLR, and EC/HDT, respectively), with the solid curves corresponding to the sum of all the emission components in each panel.

jet particles, and exceeding the mean accretion power in the source ($L_p \sim 10 L_{\text{acc}}$ and $L_p \sim 10 L_e \gg L_B$).

The above considerations should be taken with extreme caution, however, since in the modeling presented here no synchrotron data concurrent with the analyzed γ -ray flares could be utilized. Any robust estimation of the magnetic field within the emitting region would, in fact, require exactly simultaneous infrared/optical and GeV flux measurements. At the same time, we note that

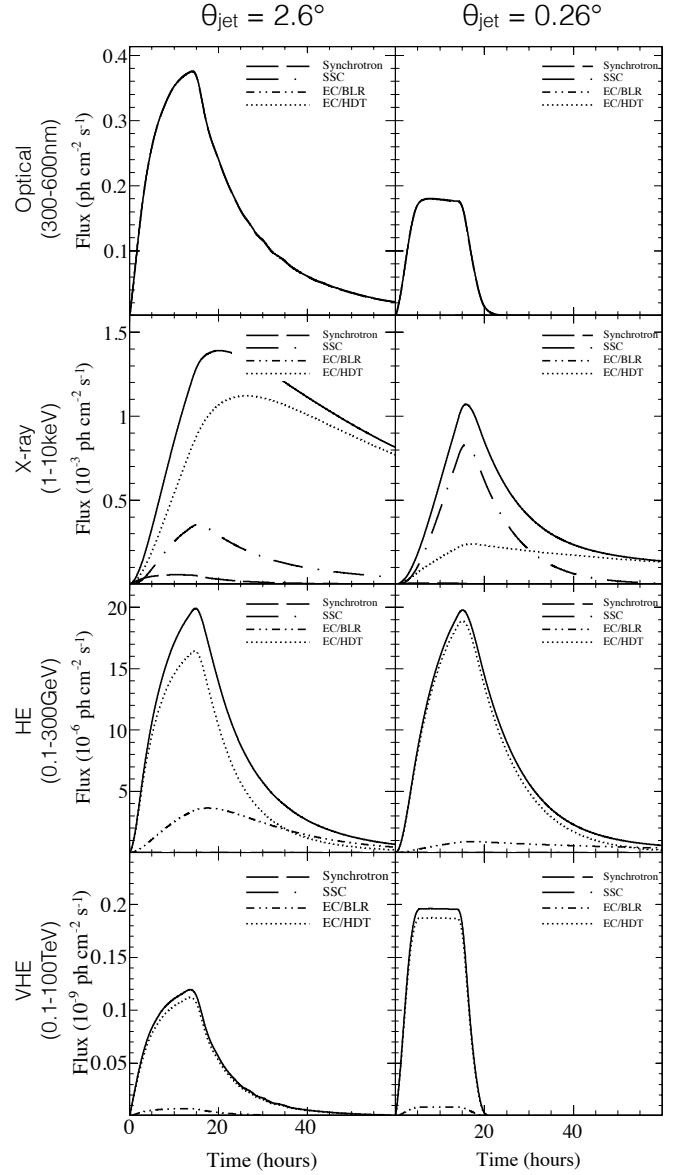


FIG. 7.— Same as Figure 6, but for Flare 2.

small jet opening angle $\Gamma \theta_{\text{jet}} < 1$ implies higher number density of the radiating electrons when compared with the case of a free-expanding jet, regardless on the jet magnetization, and therefore an elevated SSC spectral component (which may dominate the entire X-ray domain, up to even the soft γ -ray regime). Hence, high-quality X-ray data simultaneous with the GeV flaring events, when modeled as presented in this paper, could, in principle, constrain robustly the jet opening angle in the source. This is demonstrated more quantitatively in Figures 6 and 7, where we present the simulated light curves corresponding to the Flare 1 and Flare 2, respectively, in various frequency ranges, for different jet opening angles. One can see that flaring timescales become in general shorter in the case of a collimated outflow, the most pronouncedly however in the X-ray domain, which constitutes a complex superposition of the SSC and EC

emission components. Also, for the given HE γ -ray flare profile and amplitude there is a significant difference between the relative amplitudes of optical/X-ray and VHE γ -ray flares depending on the jet opening angle; in particular, in the case of $\theta_{\text{jet}} = 1/\Gamma$ the optical and X-ray flares are much more prominent when compared with a moderate increase in the VHE flux, while for $\theta_{\text{jet}} = 0.1/\Gamma$ the situation reverse.

6. CONCLUSIONS

In this paper we presented a new approach for constraining luminous blazars, incorporating fully time-dependent and self-consistent modeling of particularly bright and well-resolved γ -ray flares of PKS 1510-089 detected with *Fermi*-LAT. The two flares selected for the analysis, studied before by Saito et al. (2013), constitute the best known examples of prominent, isolated, and coherent events (with well-defined flux rising and decay phases on hourly timescales), unlike the majority of the observed blazar flux enhancements which seem rather like a superposition of distinct (though possibly related) but just unresolved sub-flaring/flickering. Unfortunately, no simultaneous data at lower (radio-to-X-ray) frequencies are available for the analyzed flares.

The results of our modeling, performed with the BLAZAR code developed by Moderski et al. (2003) in the framework of the internal shock scenario, are largely in agreement with the recent broad-band observations of FSRQs in general, and with the detection of TeV γ -ray photons correlated with the GeV flares in particular. Such a correlation, along with the apparent smoothness of the observed γ -ray spectra from 100 MeV up to the TeV range, strongly suggests a co-spatiality of the GeV and TeV emitting regions, which have to be in addition located outside the BLR in order to avoid a significant attenuation of the γ -ray fluxes due to the efficient photon-photon annihilation (see Barnacka et al. 2014). And indeed, the best-fit location of the γ -ray flaring region estimated here for PKS 1510-089 turns out as $R \simeq 0.3$ pc for a free-expanding jet with the opening angle $\theta_{\text{jet}} \simeq 1/\Gamma \simeq 2.6$ deg, up to $R \simeq 3$ pc for a collimated outflow with $\theta_{\text{jet}} \simeq 0.1/\Gamma \simeq 0.26$ deg (as advocated by Clausen-Brown et al. 2013; Jorstad et al. 2005; Zdziarski et al. 2015). This is safely beyond the characteristic scale of the BLR in the source (~ 0.03 pc).

We note that several other complementary arguments have been presented in the literature in support of the dominant blazar emission zone located at \sim pc distances from the core (see the discussion in Sikora et al. 2009; Nalewajko et al. 2014).

Under the $\Gamma\theta_{\text{jet}} \simeq 1$ assumption, our modeling in-

dicates in addition an extremely efficient jet production during the flaring events and a mixed jet content, with the dominant proton energy flux exceeding the total available accretion power in the studied blazar, $L_j \sim L_p \sim 10 L_{\text{acc}}$. This is in contrast to the quiescence states of the source, during which the $L_j \sim 0.1 L_{\text{acc}}$ condition and an approximate equipartition between different plasma constituents (protons, electrons, and magnetic field) seem to hold. In the case of a collimated jet with $\Gamma\theta_{\text{jet}} \simeq 0.1$, on the other hand, the flaring jet production efficiency decreases by an order of magnitude. Only strictly simultaneous observations of flaring PKS 1510-089 at infrared, X-ray, and GeV photon energies, augmented by fully self-consistent and time-dependent simulations as presented in this paper, may help to remove such an order-of-magnitude uncertainty, by imposing precise constraints on the magnetization and opening angle of the emitting region.

We note that the jet production efficiency L_j/L_{acc} exceeding 100% is in principle consistent with the recent understanding of the jet launching via the Blandford-Znajek process in the case when the magnetic field threading the SMBH horizon saturates at the maximum sustainable level (see Tchekhovskoy et al. 2011; McKinney et al. 2012, also the discussion in Ghisellini et al. 2014). Yet the jet magnetization emerging in our modeling is very low, so a self-consistency of the internal shock scenario explored in this paper would require in addition a very efficient conversion of the magnetic energy flux to the particle flux (accompanied by an efficient proton loading) between the jet base and the blazar emission zone (located at \sim pc distances from the core). It may be that other energy dissipation processes are involved instead in the production of blazar flares, including turbulent acceleration (e.g., Ushio et al. 2010; Lefa et al. 2011; Tramacere et al. 2011; Cao & Wang 2013; Yan et al. 2013; Asano et al. 2014; Zheng et al. 2014; Kakuwa et al. 2015; Chen et al. 2015), or relativistic magnetic reconnection (see, e.g., Narayan & Piran 2012; Giannios 2013; Sironi et al. 2015, and references therein). These interesting alternatives have been analyzed so far more quantitatively only in the context of low-power blazars of the BL Lac type, and not FSRQs, for which the internal shock scenario is still the most appealing possibility (though see in this context also the discussion in Nalewajko et al. 2012b).

L.S. was supported by Polish NSC grant DEC-2012/04/A/ST9/00083.

REFERENCES

- Abdo, A. A., Ackermann, M., Ajello, M., et al. 2009, *ApJ*, 699, 817
- Abdo, A. A., Ackermann, M., Ajello, M., et al. 2011, *ApJ*, 733, L26
- Acero, F., Ackermann, M., Ajello, M., et al. 2015, [arXiv:1501.02003v2](https://arxiv.org/abs/1501.02003v2)
- Abramowski, A., Acero, F., et al. 2013, *A&A*, 554, AA107
- Aleksić, J., Ansoldi, S., Antonelli, L. A., et al. 2014, *A&A*, 569, A46
- Asano, K., Takahara, F., Kusunose, M., Toma, K., & Kakuwa, J. 2014, *ApJ*, 780, 64
- Barnacka, A., Moderski, R., Behera, B., et al. 2014, *A&A*, 567, A113
- Blandford, R. D. & Znajek, R. L. 1977, *MNRAS*, 179, 433
- Böttcher, M., & Dermer, C. D. 2010, *ApJ*, 711, 445
- Brown, A. M. 2013, *MNRAS*, 431, 824
- Cao, G., & Wang, J. 2013, *PASJ*, 65, 109
- Cerruti, M., Dermer, C. D., Lott, B., Boisson, C., & Zech, A. 2013, *ApJ*, 771, L4
- Chen, X., Pohl, M., Boettcher, M. 2015, *MNRAS*, 447, 530
- Clausen-Brown, E., Savolainen, T., Pushkarev, A. B., et al. 2013, *A&A*, 558, A144
- Dermer, C. D., & Atoyan, A. M. 2002, *ApJ*, 568, L81

- Foschini, L., Ghisellini, G., Tavecchio, F., Bonnoli, G., & Stamerra, A. 2011, *A&A*, 530, A77
- Foschini, L., Bonnoli, G., Ghisellini, G., Tagliaferri, G., Tavecchio, F., & Stamerra, A. 2013, *A&A*, 555, A138
- Ghisellini, G., Tavecchio, F., Foschini, L., et al. 2010, *MNRAS*, 402, 497
- Ghisellini, G., Tavecchio, F., Maraschi, L., Celotti, A., & Sbarrato, T. 2014, *Nature*, 515, 376
- Giannios, D. 2013, *MNRAS*, 431, 355
- Janiak, M., Sikora, M., & Moderski, R. 2015, *MNRAS*, 449, 431
- Jorstad, S. G., Marscher, A. P., Lister, M. L., et al. 2005, *ApJ*, 130, 1418
- Kakuwa, J., Toma, K., Asano, K., Kusunose, M., & Takahara, F. 2015, *MNRAS*, 449, 551
- Kardashev, N. S. 1962, *Soviet Ast.*, 6, 317
- Kataoka, J., Madejski, G., Sikora, M., et al. 2008, *ApJ*, 672, 787
- Lefa, E., Rieger, F. M., & Aharonian, F. 2011, *ApJ*, 740, 64
- Liu, H. T., & Bai, J. M. 2006, *ApJ*, 653, 1089
- Marscher, A. P., Jorstad, S. G., Larionov, V. M., et al. 2010, *ApJ*, 710, L126
- McKinney, J. C., Tchekhovskoy, A., & Blandford, R. D. 2012, *MNRAS*, 423, 3083
- Mimica, P., & Aloy, M. A. 2012, *MNRAS*, 421, 2635
- Moderski, R., Sikora, M., & Blazewski, M. 2003, *A&A*, 406, 855
- Moderski, R., Sikora, M., Madejski, G. M., & Kamae, T. 2004, *ApJ*, 611, 770
- Moderski, R., Sikora, M., Coppi, P. S., & Aharonian, F. 2005, *MNRAS*, 363, 954
- Nalewajko, K., Sikora, M., Madejski, G., et al. 2012a, *ApJ*, 760, 69
- Nalewajko, K., Begelman, M. C., Cerutti, B., Uzdensky, D. A., & Sikora, M. 2012b, *MNRAS*, 425, 2519
- Nalewajko, K., Begelman, M. C., & Sikora, M. 2014, *ApJ*, 789, 161
- Narayan, R., & Piran, T. 2012, *MNRAS*, 420, 604
- Nolan, P. L., Abdo, A. A., Ackermann, M., et al. 2012, *ApJS*, 199, 31
- Orienti, M., Koyama, S., D'Ammando, F., et al. 2013, *MNRAS*, 428, 2418
- Rani, B., Lott, B., Krichbaum, T. P., Fuhrmann, L., & Zensus, J. A. 2013, *A&A*, 557, AA71
- Rueda-Becerril, J. M., Mimica, P., & Aloy, M. A. 2014, *MNRAS*, 438, 1856
- Saito, S., Stawarz, L., Tanaka, Y., et al. 2013, *ApJ*, 766, L11
- Sbarrato, T., Padovani, P., & Ghisellini, G. 2014, *MNRAS*, 445, 81
- Sikora, M., Begelman, M. C., & Rees, M. J. 1994, *ApJ*, 421, 153
- Sikora, M., Stawarz, L., & Lasota, J.-P. 2007, *ApJ*, 658, 815
- Sikora, M., Stawarz, L., Moderski, R., Nalewajko, K., & Madejski, G. M. 2009, *ApJ*, 704, 38
- Sironi, L., Petropoulou, M., & Giannios, D. 2015, *MNRAS*, 450, 183
- Sobolewska, M. A., Siemiginowska, A., Kelly, B. C., et al. 2014, *ApJ*, 786, 143
- Spada, M., Ghisellini, G., Lazzati, D., & Celotti, A. 2001, *MNRAS*, 325, 1559
- Stawarz, L., Sikora, M., Ostrowski, M. et al. 2004, *ApJ*, 608, 95
- Stern, B. E., & Poutanen, J. 2011, *MNRAS*, 417, L11
- Tanaka, Y. T., Stawarz, L., Thompson, D. J., et al. 2011, *ApJ*, 733, 19
- Tavecchio, F., & Mazin, D. 2009, *MNRAS*, 392, L40
- Tchekhovskoy, A., Narayan, R., & McKinney, J. C. 2011, *MNRAS*, 418, L79
- Tramacere, A., Massaro, E., & Taylor, A. M. 2011, *ApJ*, 739, 66
- Ushio, M., Stawarz, L., Takahashi, T., et al. 2010, *ApJ*, 724, 1509
- Yan, D., Zhang, L., Yuan, Q., Fan, Z., & Zeng, H. 2013, *ApJ*, 765, 122
- Zdziarski, A. A., Sikora, M., Pjanka, P., & Tchekhovskoy, A. 2015, *MNRAS*, 451, 927
- Zheng, Y. G., Kang, S. J., & Li, J. 2014, *MNRAS*, 442, 3166